Morphological and genomic shifts in mole-rat 'queens' increase fecundity but reduce skeletal integrity

Rachel A. Johnston[1*], Philippe Vullioud[2], Jack Thorley[2], Henry Kirveslahti[4], Leyao Shen[3], Sayan Mukherjee[4,5,6,7], Courtney Karner[3,8], Tim Clutton-Brock[2,9], Jenny Tung[1,10,11,12*]

[1]Department of Evolutionary Anthropology, Duke University, Durham, North Carolina 27708, USA
[2]Department of Zoology, University of Cambridge, Cambridge CB23EJ, UK
[3]Department of Orthopaedic Surgery, Duke Orthopaedic Cellular, Developmental, and Genome Laboratories, Duke University School of Medicine, Durham, NC 27710, USA
[4]Department of Statistical Science, Duke University, Durham, NC 27708, USA
[5]Department of Computer Science, Duke University, Durham, NC 27708, USA
[6]Department of Mathematics, Duke University, Durham, NC 27708, USA
[7]Department of Bioinformatics & Biostatistics, Duke University, Durham, NC 27708, USA
[8]Department of Cell Biology, Duke University, Durham, NC 27710, USA
[9]Department of Zoology and Entomology, Mammal Research Institute, University of Pretoria, 0028, Pretoria, South Africa
[10]Department of Biology, Duke University, Durham, North Carolina 27708, USA
[11]Institute of Primate Research, National Museums of Kenya, Nairobi 00502, Kenya
[12]Duke Population Research Institute, Duke University, Durham, NC 27708, USA
*Correspondence: racheljohnston7@gmail.com, jt5@duke.edu

Abstract

In some mammals and many social insects, highly cooperative societies are characterized by reproductive division of labor, in which breeders and nonbreeders become behaviorally and morphologically distinct. While differences in behavior and growth between breeders and nonbreeders have been extensively described, little is known of their molecular underpinnings. Here, we investigate the consequences of breeding for skeletal morphology and gene regulation in highly cooperative Damaraland mole-rats. By experimentally assigning dominant breeding 'queen' status versus nonbreeder status to paired littermates, we confirm that queens experience vertebral growth that likely confers advantages to fecundity. However, they also up-regulate bone resorption pathways and show reductions in femoral mass, which predicts increased vulnerability to fracture. Together, our results show that, as in eusocial insects, reproductive division of labor in mole-rats leads to gene regulatory rewiring and extensive morphological plasticity. However, in mole-rats, concentrated reproduction is also accompanied by costs to bone strength.

Introduction

A hallmark of highly cooperative societies is reproductive division of labor. This phenomenon is best understood in eusocial insects, where environmental cues lead to reproductively and morphologically specialized castes, including one or few highly fecund "queens"[1]. These changes help support the reproductive role of queens by differentiating them from nonbreeding colony members, who forage, care for young, and engage in colony defense[1,2]. Queens are frequently much larger than their sterile colony mates (e.g., twice as large in honey bees and Pharaoh ants[3,4]), reflecting dramatically altered growth and development programs that

are explained by changes in gene regulation[5]. Social insects thus exemplify the link between reproductive division of labor, cooperative behavior, and extreme morphological plasticity.

Systems in which breeding is restricted to a single female supported by multiple nonbreeding helpers are also observed in vertebrates, including birds and mammals[6]. Here, breeding status is not determined during early development, but instead occurs in adulthood, for those individuals who have the opportunity to transition into a reproductive role. In some species, new breeders undergo a period of accelerated growth, which may be important either for maintaining dominance or for supporting high fecundity[7-12]. While substantial gene regulatory divergence with breeding status has been described for the brain and some peripheral organs[13-15], we know little about the gene regulatory shifts responsible for breeder-associated growth patterns. These processes are key to understanding both the basis for, and limits of, status-driven differences in growth and development.

Here, we investigate the morphological and molecular consequences of experimental transitions to breeding status in female Damaraland mole-rats (*Fukomys damarensis*). Like naked mole-rats, Damaraland mole-rats are frequently classified as 'eusocial'[16-18], and female helpers who transition to queens experience accelerated vertebral growth associated with increases in fecundity[9,11]. However, no study has yet profiled gene regulation in mole-rat breeders and helpers in skeletal tissue, investigated their consequences for skeletal growth potential and integrity, or determined whether they extend beyond the vertebrae. To do so here, we randomly assigned littermate sisters in captive colonies to become queens or remain as nonbreeders and evaluated gene regulatory and morphological changes induced by the transition to queen status. Our results indicate that queens not only experience lengthening of their lumbar vertebrae, but also show reductions in the growth potential and structural integrity of their long bones. These changes result from increased rates of bone resorption that may increase the risk of fracture, indicating that the presence of helpers does not annul the costs of reproduction to queens. As in eusocial insects, females that acquire breeding status experience substantial morphological remodeling, associated with pathway-specific changes in gene regulation.

Results

Adaptive plasticity in the skeleton of Damaraland mole-rat queens

We randomly assigned female Damaraland mole-rats (16 sets of littermates; mean age = 19.0 ± 3.8 s.d. months at assignment; Supplementary Table 1) to either transition to queen status in a newly founded colony (n = 12) or remain as nonbreeders for the duration of the experiment (n = 18) (Figure 1A). Nonbreeders were either kept in their natal colonies as helpers or placed into solitary housing, which recapitulates extended periods of dispersal in this species[18] (n = 10 helpers and n = 8 solitaires). Six non-experimental animals (1 queen and 5 nonbreeders) were also included in the sample, resulting in a total sample size of 13 breeders and 23 nonbreeders (Supplementary Table 1).

Females assigned to the queen treatment were each transferred to a new tunnel system containing only an unrelated adult male, simulating the natural process of dispersal and new colony formation in the wild[18]. Pairing with an unrelated male leads to rapid activation of the reproductive axis, including initiation of ovulation, sexual activity, and the potential for conception[19,20]. At the start of experimental treatment, animals assigned to the queen treatment and to the nonbreeding treatment did not significantly differ in body mass (unpaired t-test, t = 0.894, df = 16.828, p = 0.384; means = 116.3 and 110.9 grams), age (unpaired t-test, t = 0.746, df = 22.137, p = 0.466; means = 628 and 580 days), or vertebral length (as measured by lumbar

vertebra 5 [LV5] following [11]; unpaired t-test, t = -1.053, df = 20.131, p = 0.305; means = 5.0 and 5.13 mm). Queens gave birth to a mean of 6.92 ± 5.57 s.d. live offspring during the 12 – 22 month follow up period, produced in a mean of 2.85 ± 1.75 s.d. litters (Supplementary Table 1).

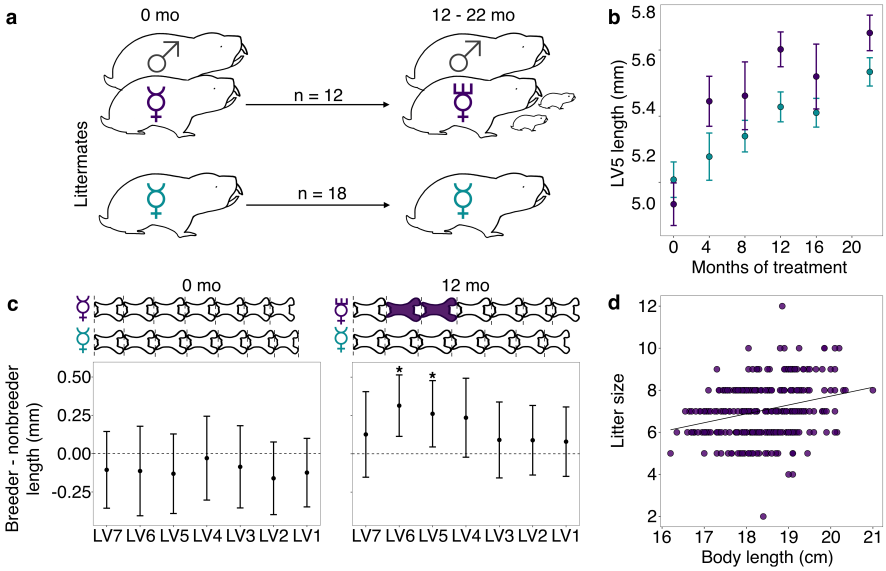

Figure 1. Transition to queen status leads to lumbar vertebral lengthening. (a) Experimental design: nonbreeding adult female (☿) littermates were randomly assigned to transition to queen status (purple ♕) by being paired with an unrelated male (♂), or to remain in a nonbreeding treatment (cyan). Duration of treatment ranged from 12 – 22 months. **(b)** Queens show more rapid growth in lumbar vertebra 5 (LV5) in the first four months of the experiment, relative to nonbreeders (treatment by time point interaction: $\beta = 0.078$, n = 49, $p = 3.47 \times 10^{-3}$). Dots show means +/- standard errors (bars). **(c)** At the start of the experiment (0 months, left panel), the lumbar vertebrae of breeders do not differ from those of nonbreeders (unpaired t-tests, all $p > 0.05$). However, at 12 months (right panel), queens have longer lumbar vertebrae relative to nonbreeders (unpaired t-tests, * indicates $p < 0.05$). Dots show means +/- standard errors (bars). Lengths of lumbar vertebrae above the plots are scaled to indicate the mean lengths of queens (top) and nonbreeders (bottom) at each time point; vertebrae highlighted in purple are significantly longer in queens relative to nonbreeders. **(d)** Litter size is positively correlated with maternal body length in the Damaraland mole-rat colony ($\beta = 0.353$, n = 328 litters, $p = 1.35 \times 10^{-3}$).

As previously described[11], queens showed rapid growth in the lumbar vertebrae in the first 12 months post-pairing, relative to nonbreeders (Figure 1B). In contrast to naked mole-rats, where the lumbar vertebrae at the cranial end exhibit the most growth in queens[21], the lumbar vertebrae toward the caudal end (LV5 and LV6) were most responsive to breeding status in our experiment, suggesting potential convergent evolution of the vertebral lengthening phenotype. Based on longitudinal measurements, most of this differential growth was concentrated soon after the breeding status transition, concordant with findings in naked mole-rats[22]. Specifically, we observed a significant interaction between breeding status (queen versus nonbreeder) and post-pairing time point in the first four months of the experiment (Figure 1B; $\beta = 0.0784$, $p = 3.47 \times 10^{-3}$; n = 49 x-rays from 28 animals), but not for x-rays taken in later time point intervals (4 months versus 8 months; 8 versus 12 months, all $p > 0.05$). However, due to the early increased growth in queens, size differences persisted, such that the absolute length of LV5 in queens was, on average, 4.8% longer than nonbreeders after 12 months (Figure 1C; LV5: unpaired t-test, t = 2.509, df = 21.095, p = 0.020), and the absolute length of the lumbar vertebral column in queens relative to nonbreeders was 3.5% longer, although the latter difference was not significant (unpaired t-test, t = 1.945, df = 22.49, p = 0.064). Differences between queens and nonbreeders were even more apparent if lumbar vertebrae measures were scaled by zygomatic

126 arch (head) width, as done in previous studies[9,11,22] (LV5: 9.3% longer, unpaired t-test, t = 4.12,
127 df = 15.135, p = 8.87 x 10^{-4}; lumbar vertebral column length: 7.9% longer, unpaired t-test, t =
128 4.34, df = 15.37, p = 5.58 x 10^{-4}). This difference highlights changes in allometry across the
129 queen skeleton due to the combination of lumbar vertebral growth and narrower zygomatic arch
130 width in queens (4% narrower at 12 months, unpaired t-test, t = -2.448, df = 24.126, p = 0.022).
131 Consistent with previous results[11], queens in the colony with longer bodies (which
132 correlates with longer lumbar vertebrae, Pearson's *r* = 0.856, p = 5.99 x 10^{-59}; Supplementary
133 Figure 1) had more pups per litter (Figure 1D; Supplementary Table 2; β = 0.353, p = 1.35 x 10^{-3},
134 n = 328 litters from all breeding groups maintained in the same breeding facility). Controlling for
135 litter size, longer queens also had larger pups: for every additional centimeter of maternal body
136 length, pup body mass increased by 2.9% (β = 0.28, p = 0.032, n = 971 pups). Thus, the
137 elongated queen phenotype is a strong candidate for adaptive plasticity that supports increased
138 fertility in queen mole-rats.
139
140 **Breeding status induces gene regulatory changes in the queen mole-rat skeleton**
141 To identify the gene regulatory changes associated with skeletal plasticity, we cultured
142 cells enriched for bone marrow-derived mesenchymal stromal cells (bMSCs) isolated from the
143 lumbar vertebrae (pooled LV1-LV5) of both queens and nonbreeders (n = 5 queens, 11
144 nonbreeders). bMSC cultures include multipotent skeletal stem cells, the precursor of the
145 osteoblast and chondrocyte lineages responsible for bone growth. In parallel, we cultured cells
146 enriched for bMSCs from the pooled long bones (humerus, ulna, radius, left femur, and left tibia)
147 of the same animals, which do not show increased elongation in queens (for both tibia length and
148 femur length, all p > 0.05 for interactions between breeding status and time intervals [0 months
149 versus 4 months, 4 months versus 8 months, 8 months versus 12 months]; femur at 12 months:
150 unpaired t-test, t = -0.202, df = 19.326, p = 0.842; tibia at 12 months: unpaired t-test, t = -0.860,
151 df = 16.759, p = 0.402). To evaluate the potential role of sex steroid hormone signaling on bone
152 growth, we treated cells from each bone sample for 24 hours with either 10 nM estradiol or
153 vehicle control, resulting in 47 total samples. We then performed RNA-seq on each sample to
154 screen for genes that were systematically differentially expressed in the bone cells of queens
155 versus nonbreeders.
156 Of 10,817 detectably expressed genes, 171 genes showed a significant effect of breeding
157 status at a false discovery rate (FDR) threshold of 10% in the long bones (329 at an FDR of 20%;
158 Supplementary Table 3). Surprisingly, no genes showed a significant effect of breeding status in
159 the lumbar vertebrae at either FDR threshold. However, effect sizes were highly correlated
160 between bone types overall (R^2 = 0.75, p = 4.60 x 10^{-53}), with more pronounced effects of
161 breeding status in the long bone samples than in the lumbar vertebrae (paired t-test on breeding
162 status effects in long bone versus vertebrae: t = 3.97, df = 317.67, p = 8.73 x 10^{-5}). Importantly,
163 breeding status-related differences were not readily attributable to differences in bone cell
164 composition. Based on both canonical markers of bMSC lineage cells and deconvolution of the
165 RNA-seq data using data from 27 mesenchymal or hematopoietic lineage mouse cell types, the
166 majority cell type in both queen and nonbreeder samples was most similar to cells from the
167 bMSC lineage[23-25] (Supplementary Figures 2 and 3). Additionally, estimated cell type
168 proportions (as summarized by the top three principal components) did not differ between
169 queens and nonbreeders (all FDR > 0.1, Supplementary Table 4), and we identified no cases in
170 which the effects of breeding status on gene expression were significantly mediated by the first
171 principal component of cell composition (p > 0.05 for all 171 queen-associated genes at 10%

FDR; Supplementary Table 5). Because we observed no significant effect of estradiol treatment on gene expression in either bone type (all FDR > 10%), we did not evaluate the effects of estradiol further.

The majority of breeding status-associated genes were up-regulated in queens (151 of 171 genes, 88%). In support of their role in skeletal plasticity, up-regulated genes were enriched for "bone remodeling" ($\log_2$[OR] = 4.07, p = 5.07 x 10^{-6}), a process that involves the balanced cycle between bone formation by osteoblasts and bone resorption by osteoclasts[26] (Figure 2). Surprisingly, however, enriched terms were specifically concentrated in pathways and processes related to bone resorption, not formation (Supplementary Table 6), including "positive regulation of bone resorption" (Figure 2A, C; $\log_2$[OR] = 6.51, p = 1.55 x 10^{-6}) and "superoxide anion generation" (Figure 2A, C; $\log_2$[OR] = 5.29, p = 1.4 x 10^{-5}), which is involved in osteoclast activity and degradation of bone matrix[27-30]. Differentially expressed genes were also enriched for immune-related processes (e.g., "cytokine secretion", "chemotaxis", "leukocyte activation involved in immune response"; Supplementary Table 6). These observations suggest that transitions to queen status also involve changes in immunoregulatory signaling (osteoclast cells, like macrophages, are derived from monocytes). Omni-ATAC-seq profiling of open chromatin regions further supports a central role for bone resorption and osteoclast activity in the queen skeleton (n = 8; Supplementary Table 7). Specifically, transcription factor binding motifs (TFBMs) located in accessible chromatin near queen up-regulated genes were enriched for PU.1 and MITF, two transcription factors that are essential for osteoclast differentiation[31] (Figure 2B, C; PU.1 $\log_2$[OR] = 1.041, p = 2.84 x 10^{-4}; MITF $\log_2$[OR] = 0.707, p = 7.36 x 10^{-3}; see Supplementary Table 7 for complete list of enriched TFBMs). *MITF* was also among the 151 genes that were differentially expressed between queens and nonbreeders and up-regulated in both queen long bones and lumbar vertebrae.

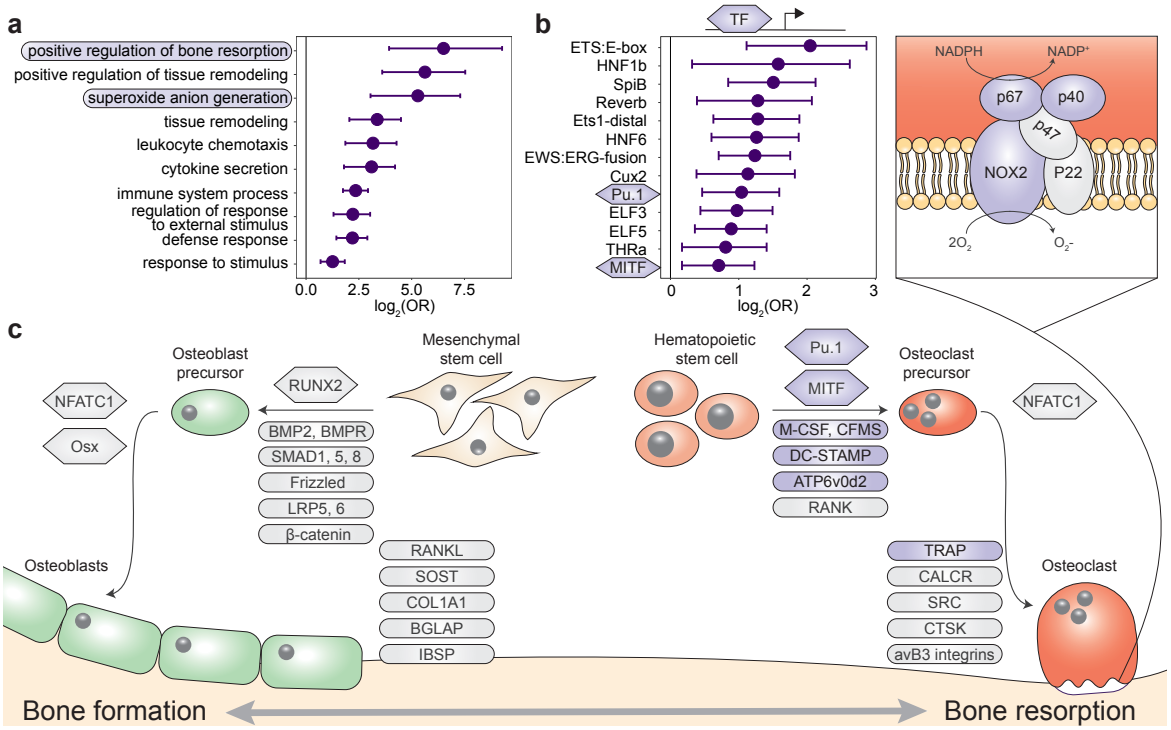

Figure 2. Queen status drives increased regulatory activity of bone resorption pathways. (a) Gene Ontology (GO) terms enriched in queen up-regulated genes, relative to the background set of all genes tested. Bars represent 95% confidence intervals. Processes highlighted in purple are also depicted in (c). Highest-level (most general) terms are shown; for full GO enrichment results, see Supplementary Table 6. **(b)** Accessible transcription factor binding site motifs enriched near queen up-regulated genes, relative to all genes tested. Bars represent 95% confidence intervals. Transcription factors highlighted in purple are also depicted in (c). **(c)** Schematic of the balance between bone formation and bone resorption, showing key regulators and markers for mesenchymal stem cell differentiation into osteoblasts and hematopoietic stem cell differentiation into osteoclasts[26,31]. Queen up-regulated genes or proteins are highlighted as purple ovals (FDR < 10%) and transcription factors with binding motifs enriched near queen up-regulated genes are highlighted as purple hexagons. Inset for osteoclasts shows the NADPH oxidase system, which generates superoxide radicals (O_2^-) necessary for bone resorption and is highly enriched for queen up-regulated genes (purple ovals).

Extensive skeletal remodeling in queen mole-rats

The gene expression data suggest that queen status-driven changes to the skeleton extend beyond the lumbar vertebrae to the long bones. Further, they suggest that bone resorption—an important counterpoint to bone formation that is required for normal skeletal maintenance—also distinguishes breeding and nonbreeding females. To investigate this possibility, we performed high-resolution micro-computed tomography (μCT) scanning to generate 3D reconstructions of LV6, LV7, right femur, and right tibia of queens and female nonbreeders (n = 140 bones from 36 animals; Figure 3A; Supplementary Figure 4). This approach substantially increases the level of resolution for investigating breeding status-linked differences in skeletal morphology, as previous studies relied on x-ray data alone[9,11].

We first asked whether breeding status could be predicted from morphological differences in the 3D reconstructions. We found that it could for the lumbar vertebra, but not for the femur: by applying the smooth Euler characteristic transform[32], we were able to predict queen versus nonbreeder status in LV6 (77.8% accuracy, p = 0.01, n = 36), but not the femur (52.8% accuracy, p = 0.53, n = 36). Including only highly fecund queens (≥6 total offspring)

224 improved predictive accuracy in the femur (70% accuracy, $p = 0.12$, $n = 30$). Although these
225 predictions did not reach statistical significance, they raised the possibility that morphological
226 changes in femurs become enhanced with increasing reproductive effort.
227 We next tested whether the transition to queen status affects the ability to continue bone
228 lengthening. Lengthening requires the presence of a growth plate, a region of cartilage in the
229 bone where longitudinal growth occurs through proliferation of cartilage cells (chondrocytes)
230 (Figure 3A-B; Supplementary Figure 4). Closure of the growth plate, which indicates that bone
231 lengthening potential has terminated, typically occurs in mammals after reaching sexual
232 maturation, when energy begins to be invested in reproduction instead of growth[33]. To test
233 whether the transition to queen status alters bone lengthening potential, we performed Safranin-
234 O staining on sections of the right tibia and LV7 to visualize growth plates (Figure 3B). In the
235 proximal tibia but not LV7, queens were less likely to have open growth plates (Figure 3C;
236 Supplementary Figure 4; Supplementary table 8; tibia: two-sided binomial test, $p = 0.019$; LV7:
237 two-sided binomial test, $p = 0.422$). The increased probability of growth plate closure in the tibia
238 of queens is linked to the number of offspring a female has produced: females with more
239 offspring showed a higher expanse of closure across the growth plate ($\beta = 0.050$, $p = 4.51 \times 10^{-3}$,
240 $n = 12$, controlling for age). This pattern may be due in part to reduced chondrocyte proliferation,
241 as females that produced more offspring had fewer chondrocyte columns in the remaining
242 growth plate (Figure 3D; $\beta = -0.132$, $p = 0.020$, $n = 12$, controlling for age). Thus, offspring
243 production in queens is associated with loss of the ability to lengthen the long bones, but not the
244 lumbar vertebrae, consistent with the importance of abdominal lengthening for supporting larger
245 litters.

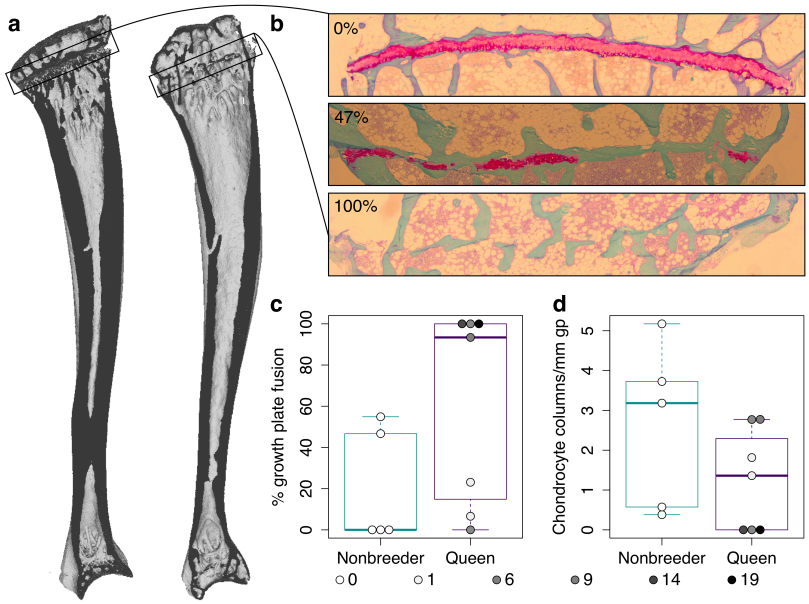

246 **Figure 3. Queen status reduces growth potential in the tibia. (a)** µCT scans of female Damaraland mole-rat tibias. Boxes
247 indicate the location of the proximal growth plate, which is either unfused (left) or fully fused (right). **(b)** Example Safranin-O
248 stained histological sections of the proximal tibia, in which the growth plate is unfused (top), partially fused (middle), or fully
249 fused (bottom). Values in the top left of each box indicate percent growth plate fusion across the width of the bone. The
250 cartilaginous growth plate is stained deep pink and calcified bone is stained green. **(c)** Queens, and specifically queens that gave
251 birth to more offspring, show increased growth plate fusion ($\beta = 0.050$, $p = 4.51 \times 10^{-3}$, $n = 12$, controlling for age) and **(d)**
252 decreased number of chondrocyte columns within the remaining growth plate ($\beta = -0.132$, $p = 0.020$, $n = 12$, controlling for age).
253 Each box represents the interquartile range, with the median value depicted as a horizontal bar. Whiskers extend to the most
254 extreme values within 1.5x of the interquartile range. In (c) and (d), dots represent individual animals, and shading indicates each
255 animal's total offspring number. Ages of queens and nonbreeders do not significantly differ (unpaired t-test, $t = 0.489$, $n = 12$, $p =$
256 0.644).

A major demand on reproductively active female mammals is a high requirement for calcium, particularly during lactation when mothers support rapid offspring bone growth. Maternal skeletons are remodeled to meet this demand, although in most mammals, these changes are not permanent (reviewed in [34]). Because of the particularly intense reproductive investment made by cooperatively breeding mole-rat queens, we therefore also evaluated the effect of queen status on trabecular and cortical bone volumes, which are thought to be important in satisfying short-term and long-term calcium demands, respectively. We found no effect of queen status on the amount of trabecular bone in the femur, tibia, LV6, or LV7 (all $p > 0.05$ for bone volume/total volume). However, we found that cortical bone was significantly thinner at the femoral midshaft, but not in the lumbar vertebrae, in queens compared to their nonbreeding sisters (Figure 4A; Supplementary Figure 5; femur: paired t-test of cortical area/total area, $t = -4.067$, $df = 8$, $p = 3.60 \times 10^{-3}$; LV6: paired t-test of cortical area/total area, $t = -0.741$, $df = 6$, $p = 0.487$). Cortical thinning in queens appears to be specifically due to increased bone resorption, which typically occurs on the endosteal (internal) surface of long bones in the marrow cavity. Indeed, queens had a larger marrow cavity (paired t-test, $t = 5.355$, $df = 8$, $p = 6.82 \times 10^{-4}$; Figure 4B) but showed no difference in periosteal area compared to their nonbreeding sisters (paired t-test, $t = 1.539$, $df = 8$, $p = 0.162$; Figure 4C).

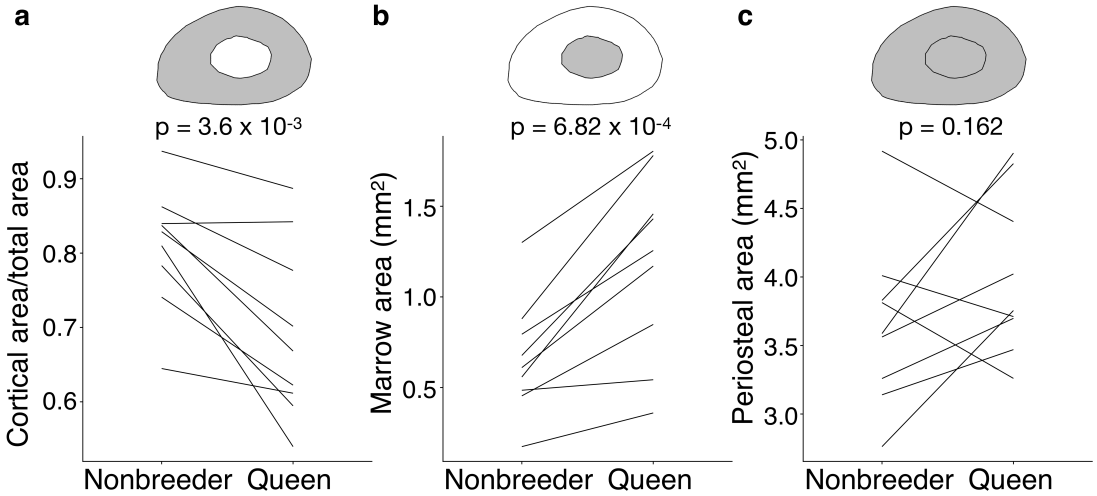

Figure 4. Queens exhibit reduced cortical area and increased marrow area at the femoral midshaft. Femoral cross-sections with area highlighted in gray show the measures represented in the corresponding plots below. Each line represents an age-matched, nonbreeder and queen littermate pair. **(a)** Queens have less cortical bone (relative to the total area of the femoral midshaft cross-section), compared to their paired nonbreeding littermates (paired t-test of cortical area/total area, $t = -4.07$, $df = 8$, $p = 3.60 \times 10^{-3}$). **(b)** Queens also have enlarged marrow cavities (paired t-test, $t = 5.36$, $df = 8$, $p = 6.82 \times 10^{-4}$), where bone resorption typically occurs, but **(c)** show no difference in overall periosteal area (paired t-test, $t = 1.54$, $df = 8$, $p = 0.162$).

Because changes in cortical bone are thought to reflect accumulated demands over long time frames, we hypothesized that cortical thinning in queens is a consequence of repeated cycles of pregnancy and lactation over time, which can occur simultaneously in Damaraland mole-rat queens. In support of this idea, we found that, within queens, the relative amount of cortical bone is not predicted by the number of pups in a queen's most recent litter ($\beta = -0.024$, $n = 13$, $p = 0.287$), but instead by the total number of pups she produced in her lifetime. Specifically, queens who had more live births had reduced cortical bone thickness along the entire shaft of the femur (Figure 5 and Supplementary Table 9; across decile sections of the femur: all $p < 0.05$, controlling for mother's litter as a random effect; at midsection: $\beta = -0.011$, $n = 13$, $p = 0.031$). Thus, cortical thinning does not commence with the transition to queen status

291 *per se* (i.e., it is not a correlate of *achieving* breeder status), but instead appears to be a
292 consequence of repeated investment in pregnancy and lactation. Notably, thinning is particularly
293 marked in queens who had at least six offspring, which usually occurs by 14 months after a
294 breeding status transition (i.e., by the third litter; Supplementary Table 9). Given that wild
295 Damaraland mole-rat queens can maintain their status for many years[35], our results suggest that
296 long-lived queens may experience substantial morphological change.

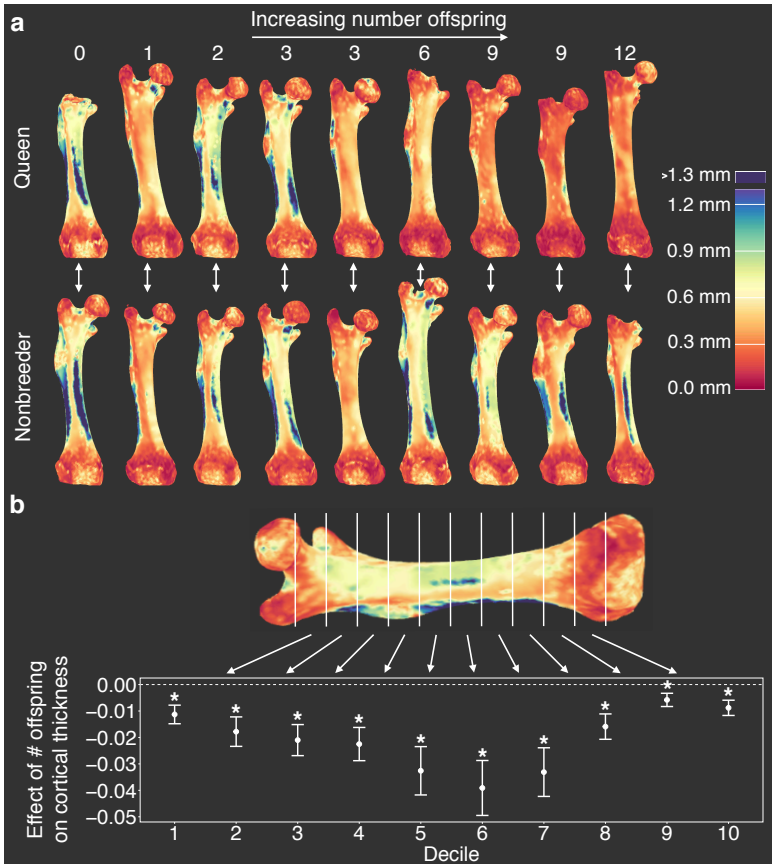

297 **Figure 5. Offspring production in queens leads to cortical thinning across the femoral shaft. (a)** Queens (top row) relative to
298 their same-aged nonbreeding littermates (bottom row) present thinner cortical bone across the femur, particularly in females that
299 have many offspring (top right). Number of offspring is indicated above each femur, and vertical arrows indicate littermate pairs.
300 **(b)** Within each decile section across the femoral shaft, number of offspring is negatively correlated with average cortical
301 thickness (linear mixed model with littermate pair as random effect). Full results are presented in Supplementary Table 9.
302 Asterisk indicates $p < 0.05$.
303

304 **Skeletal remodeling predicts increased risk of femur breakage in queens**

305 In humans, accelerated bone resorption is a central cause of osteoporosis-related bone
306 fragility[36]. We therefore hypothesized that cortical thinning in queen mole-rat femurs would be
307 linked to decreased bone strength. To test this hypothesis, we calculated two key indicators of
308 femoral structural integrity: cortical area (CA) and the minimum moment of inertia (I_{min}, a
309 predictor of resistance to bending). In nonbreeders, both are positively correlated with body mass
310 (I_{min}: $R^2 = 0.368$, $n = 24$, $p = 9.92 \times 10^{-4}$; CA: $R^2 = 0.407$, $n = 24$, $p = 4.80 \times 10^{-4}$). However, in
311 queens, I_{min} is not significantly predicted by body mass ($R^2 = 0.088$, $n = 13$, $p = 0.17$), but is
312 instead a function of number of offspring produced ($R^2 = 0.283$, $p = 0.035$). Queen CA is
313 predicted by both offspring number and body mass, but offspring number explains almost twice
314 the variance (offspring number $R^2 = 0.634$, $p = 6.83 \times 10^{-4}$; body mass $R^2 = 0.385$, $p = 0.014$).

To evaluate the effects of reproductive activity on the risk of bone failure, we drew on data on the relationship between CA and bone mechanical failure in a large data set of mouse femurs[37]. In this data set, CA is the best predictor of maximum load (the maximum force a bone can withstand prior to failure), and, crucially, the CA-max load relationship is highly linear (Supplementary Figure 6; $R^2 = 0.88$, $p = 6.64 \times 10^{-38}$). Scaling the mole-rat CA data to mouse suggests that transitions to queen significantly increase the risk of bone failure (Figure 6A; hazard ratio (95% confidence interval) = 2.67 (1.20, 5.93), n = 36, p = 0.016). Similar to growth potential and cortical thinning, this effect is driven by highly fertile queens, such that those who had at least six offspring showed the highest predicted risk of bone failure (Figure 6B; queens with ≥ 6 offspring relative to nonbreeders: HR = 3.81 (1.47, 9.83), n = 30, p = 0.006). The risk of bone failure is thus predicted to increase by 21% for each additional pup (HR = 1.21 (1.10, 1.33), n = 36, $p = 8.85 \times 10^{-5}$).

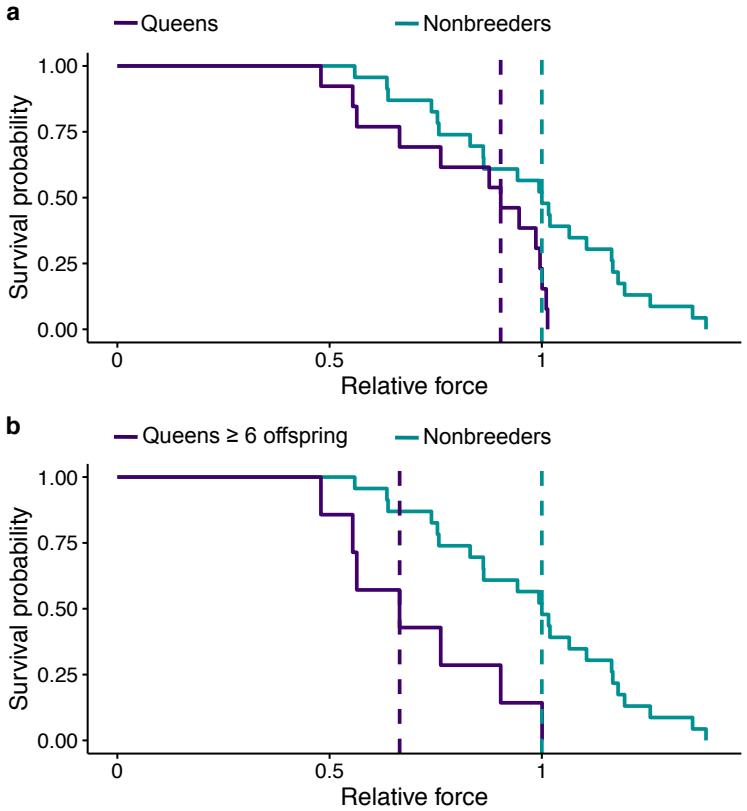

Figure 6. Effect of reproductive status on the probability of bone failure. (a) Survival curves for femurs from queens versus nonbreeders, based on predictions from the midshaft cortical area and data from [37] (Wald test, p = 0.02, n = 36; see Methods). **(b)** Survival curves for femurs from queens with ≥ 6 offspring versus nonbreeders (Wald test, p = 0.006, n = 30). Vertical dashed lines indicate group medians, with the median failure time for nonbreeders fixed at a value of 1.

Discussion

Our results demonstrate that transitions to breeding status in Damaraland mole-rat queens drive widespread skeletal remodeling linked to shifts in gene regulation. In addition to previously described vertebral growth[11], queen Damaraland mole-rats up-regulate bone resorption-related pathways, lose bone lengthening potential in the long bones, and develop thinner femurs that are predicted to be more prone to mechanical failure. While vertebral growth is triggered immediately after transition to queen status, these other changes are a function of repeated offspring production. Thus, queens quickly progress from traits typically associated with pre-

reproductive and pubertal growth in mammals (e.g., body elongation), to traits typically linked to aging (e.g., marrow cavity expansion and cortical thinning). This progression is supported by the signature of bone resorption rather than bone growth at the time of sampling, which occurred 1 – 2 years post-transition. Combined, these results suggest some key differences between Damaraland mole-rats and eusocial insects. Specifically, while abdominal lengthening allows queen mole-rats to increase fecundity per reproductive effort, loss of cortical bone in the femur is unlikely to directly benefit either fertility or survival. Instead, it reflects the cumulative burden of continuous cycles of pregnancy and lactation[34]. Thus, unlike eusocial insect queens[38,39], Damaraland mole-rat queens incur morphological costs to concentrated reproduction in addition to morphological changes that facilitate increased fitness.

The typical mammalian pattern of bone remodeling, in which bone mineral density decreases during pregnancy and lactation but recovers after offspring are weaned[34], may explain bone thinning in Damaraland mole-rats queens: queens often lactate for one litter while gestating another, leaving little to no time for recovery. One possible reason that this fast rate of breeding is achievable is that queens in colonies with more helpers work less and rest more[40], consistent with studies in other cooperative mammals that show that helpers alleviate breeding-associated loss of condition in queens[41]. However, the extent to which helpers reduce the costs of breeding to queens may differ between species depending on the relative numbers of helpers to breeders. For example, in eusocial insects, large colonies and the high ratio of helpers to queens reduce the costs of reproduction to queens to low levels[1,2]. Similarly, in naked mole-rats (where colonies can include hundreds of animals, compared to up to dozens in Damaraland mole-rat colonies[17,18,43]), a small sample of queens (n = 6) suggests increased rather than decreased femoral cortical thickness relative to age-matched nonbreeders[44]. Testing how the costs and benefits of reproduction are resolved across different levels of cooperativity, including the molecular mechanisms that mediate these differences, is an important next step towards understanding the evolution of cooperative breeding in mammals.

Acknowledgements

We thank Tim Vink, Dave Gaynor, and the mole-rat house staff and volunteers for their tremendous contributions to the Kalahari Mole-rat Project. We also thank Irene Garcia, Mari Cobb, Brianna Bowman, Anna Luiza Wolf, Alice Zhou, Yilin Yu, B.J. Nielsen, and Tawni Voyles for their contributions to sample collection and data generation, Graham Treece for guidance on quantifying bone thickness with Stradview, Karl Jepsen for sharing data on mouse femurs, Lou DeFrate for guidance on estimating bone strength, and members of the Tung lab for feedback on earlier versions of this manuscript. Support for this work was provided by the European Research Council (Grants 294494 and 742808 to T.C.B), the Human Frontier Science Program (RGP0051-2017 to J.T., S.M., and T.C.B.), the National Science Foundation (IOS-7801004 to J.T.), the National Institutes of Health (F32HD095616 to R.A.J.), a Sloan Foundation Early Career Research Fellowship to J.T., a Foerster-Bernstein Postdoctoral Fellowship to R.A.J., and a Natural Environmental Research Council Doctoral Training Program to Ja.T. High-performance computing resources were supported by the North Carolina Biotechnology Center (Grant Number 2016-IDG-1013).

Author Contributions

Conceptualization, R.A.J., T.C.B., and J.T.; Investigation, R.A.J., Ja.T., P.V., H.K., L.S., S.M., C.K., T.C.B., and J.T. Formal Analysis, R.A.J., H.K., S.M.; Writing—Original Draft, R.A.J. and

J.T.; Writing—Reviewing & Editing, R.A.J., P.V., Ja.T., H.K., L.S., S.M., C.K., T.C.B., and J.T. Funding Acquisition, J.T. and T.C.B. Supervision, T.C.B. and J.T.

Competing Interests

The authors declare no competing interests.

Methods

Study system and experimental design

Damaraland mole-rats (*Fukomys damarensis*) were maintained in a captive colony at the Kuruman River Reserve in the Northern Cape Province of South Africa, within the species' natural range. Only animals born in captivity, with known birthdates and litter composition, were used in this study. Animals were maintained in artificial tunnel systems built from PVC pipes with compartments for a nest-box and waste-box and transparent windows to allow behavioral observation. Animals were fed *ad libitum* with sweet potatoes and cucumbers.

Adult females were randomly assigned to be either nonbreeders or queens, such that females assigned to queen status had matched siblings who were assigned to the nonbreeding condition (age-matched littermates where possible). Nonbreeders were either maintained in their natal colony as helpers or maintained alone, which models the social condition experienced by dispersing females. Females assigned to the breeder condition were transferred to a new tunnel system with an unrelated male from a separate social group. Ten new breeding colonies, with corresponding age-matched nonbreeding littermates where possible (6 helper and 8 solitaire age-matched littermates, and 4 non-littermate helpers), were set up in December 2015-June 2017[11]. With one exception (G10F026), animals maintained their breeding status for 14-22 months before sample collection. Breeding females were at different stages of pregnancy at time of sacrifice. An additional 4 breeding colonies (with 4 matched littermate helpers) were formed in October 2017 and followed for 11-12 months (Supplementary Table 1). One queen died before sample collection, and one non-experimental helper was euthanized during the course of the study and included in sample collection. The final sample size included 13 breeders, 15 helpers, and 8 solitaire females.

X-ray data

For a subset of study subjects, full body X-rays were taken every two months during the first 12 months of the experiment and at the time of sacrifice. From these X-rays, an experimenter blind to animal breeding status measured the length of each lumbar vertebra from vertebra 1 to 7, the right femur, the right tibia, body length, and the width of the zygomatic arch using ImageJ[45]. The caudal-most lumbar vertebra was labeled as LV7. We tested for an effect of breeding status on LV5 using a linear mixed model in which post-pairing time point, breeding status, and the interaction of time point by breeding status were modeled as fixed effects and animal ID as a random effect.

Effects of queen body length on fertility

To test the effect of maternal body length on litter size and pup size, we used body length measurements obtained during routine colony monitoring of all queens maintained in the captive colony (i.e., not restricted to experimental animals). Following [11], we used body length measurements obtained nearest to, and no more than 90 days from, the date of parturition. The resulting dataset included 328 litters (971 pups) from 76 mothers (a 76% increase from the data

set in Thorley *et al*, 2018). We fit two linear mixed effects models. In the first model, we modeled litter size as a function of maternal body length, controlling for whether the litter was the female's first litter, and included maternal ID as a random effect. In the second model, we modeled pup mass as a function of maternal body length, controlling for litter size and whether the litter was the female's first litter as fixed effects, and maternal ID and litter ID as random effects.

Sample collection and cell culture from lumbar vertebrae and long bones

Animals were deeply anesthetized with isoflurane and sacrificed with decapitation following USGS National Wildlife Health Center guidelines and under approval from the Animal Ethics Committee of the University of Pretoria. Immediately upon sacrifice, the lumbar vertebrae and long bones were dissected, and attached muscle tissue was removed with forceps. Lumbar vertebrae 6 and 7 and the right femur and tibia were collected into 50% ethanol for 24 hours, then transferred to 70% ethanol and stored at 4° C for μCT scans and histochemistry.

To isolate bone cells for culture, lumbar vertebrae 1-5 were incubated in 2% Collagenase P (Roche, Switzerland) for 30 minutes at 30° C. Each bone was then cut in half and transferred to a 1.5 ml microcentrifuge tube containing a G-Tube microcentrifuge tube (VWR, Radnor, PA, USA) that had been punctured at the bottom with a 15 gauge needle. Tubes were spun at 3,000 RCF for 5 seconds, allowing the marrow to collect into the 1.5 mL microcentrifuge tube. Cell pellets were resuspended in red blood cell lysis buffer, pooled, and incubated for 3 minutes at room temperature. 10 ml bMSC media (MEM-alpha [ThermoFisher, Waltham, MA, USA] + 15% fetal bovine serum [Hyclone, Logan, UT, USA] + 1% penicillin/streptomycin + 2 ng/ml recombinant human fibroblast growth factor-basic [Biocam, Centurion, Gauteng, South Africa] + 10 nM ROCK inhibitor Y-27632 [RI; Cayman Chemical, Ann Arbor, MI, USA]) was added to stop lysis, and the tubes were spun for 5 minutes at 300 RCF. The cell pellet was resuspended in 1 ml bMSC media and strained through a 70 μm cell strainer. Cells were plated at 1.6 x 10^5 cells per cm^2. The long bones (excluding right femur and tibia) were processed to enrich for bMSCs following the same procedure, but without incubation in Collagenase P. Cells were cultured at 37° C and 5% CO_2. Twenty-four hours post plating, plates were carefully washed three times with 1x PBS and supplied with fresh media to remove non-adherent cells. Once bMSC clusters were visible (2-9 days post plating), plates were fed bMSC media without RI or fed bMSC media without RI + 10 nM estradiol (E2). Twenty-four hours later, cells were collected into buffer RLT and stored at -80° C. Samples were shipped on dry ice to Duke University for RNA extraction using the Qiagen RNeasy Micro Kit. RNA-Seq libraries were generated using the NEBNext Single Cell/Low Input RNA Library Prep Kit for Illumina.

Gene expression analysis

RNA-Seq libraries were sequenced on an Illumina HiSeq 4000 (100 base pair single end reads) to a mean coverage of 16.1 ± 3.9 s.d. million reads. Reads were trimmed with *cutadapt* version 2.3[46] (parameters: -q 20 -e 0.2 --times 5 --overlap 2 -a AGATCGGAAGAGC -a "T" --minimum-length=20). Trimmed reads were then mapped to the Damaraland mole-rat v1.0 genome[47] (DMR_v1.0) using two pass mapping with STAR[48]. Only uniquely mapped reads were retained. HTseq[49] was used to quantify read counts mapping to genes (using the v1.0.92 gtf file from Ensembl; we extended the genomic coordinates of the *SERPINE1* gene by 2000 basepairs in both directions due to very high expression directly adjacent to the annotated coordinates). We transformed read counts to transcripts per million (TPM)[50], and retained only genes with TPM ≥

478 2 in at least 25% of samples. We performed voom normalization[51] on the raw counts, using
479 normalization factors produced by the trimmed mean of M-values (TMM) method[52] in DESeq[53].
480 We used the *limma*[54] function *lmFit* to regress out the proportion of uniquely mapped reads in
481 genes (which controls for efficiency of mRNA selection during RNA-Seq library preparation)
482 and animal natal colony (which controls for littermate sets and date of sacrifice) to obtain
483 normalized, batch-corrected gene expression values for downstream analysis. We used the mixed
484 effects model approach in *emmreml*[55] to estimate, for each gene, the effect of breeding status on
485 gene expression within lumbar vertebrae and within long bones using the following model:
486

$$y_i = \mu + d_i\beta_1 + b_i\beta_2 + q_i\beta_3 * I(b = 0) + q_i\beta_4 * I(b = 1) + s_i\beta_5 * I(b = 0) + s\beta_6 * I(b = 1) + Zu + \varepsilon_i,$$

487

$$u \sim MVN\ 0, \sigma_u^2 K,$$
$$\varepsilon \sim MVN\ 0, \sigma_e^2$$

488
489 where y is the vector of gene expression levels for $n = 47$ samples (indexed by i); μ is the
490 intercept; d is the number of days in culture and β_1 its effect size; b is bone type (i.e., long bones
491 or lumbar vertebrae) and β_2 its effect size; and q is a 0/1 variable representing breeder status and
492 β_3 and β_4 its effect size in long bones and lumbar vertebrae, respectively. I is an indicator
493 variable for bone type (0 = long bone; 1 = lumbar vertebrae). s is a 0/1 variable representing
494 whether the cells were cultured with estradiol and β_5 and β_6 are its effect sizes in long bones and
495 lumbar vertebrae, respectively. Z is an incidence matrix that maps samples to animal ID to take
496 into account repeated sampling from the same individual, and u is a random effect term that
497 controls for relatedness. K is an m by m matrix of pairwise relatedness estimates (derived from
498 the genotype data described below) between all m animals. ε is the residual error, σ_u^2 is the
499 genetic variance component, and σ_e^2 is the environmental variance component. To control for
500 multiple testing, we calculated the false discovery rate following Storey and Tibshirani[56] using
501 an empirical null distribution derived from 100 permutations of each variable of interest.
502 We used g:profiler[57] to perform gene ontology enrichment analysis of the genes up-
503 regulated with queen status in lumbar vertebrae and long bones (151 of 171 genes significantly
504 associated with queen status at a 10% FDR). All genes in the original analysis set were used as
505 the background gene set. We set both the minimum size of the functional category and the
506 minimum size of the query/term intersection to 3. Finally, we retained categories that passed a
507 Bonferroni corrected p-value of 0.05.
508
509 **Genotyping to estimate relatedness**
510 To control for relatedness when modeling the gene expression data, we performed single
511 nucleotide polymorphism (SNP) genotyping of the RNA-Seq data using the Genome Analysis
512 Toolkit[58] (GATK). We used the SplitNCigarReads function on the trimmed, uniquely mapped
513 reads and performed GATK indel realignment. Base recalibration was performed by using all
514 SNPs with GQ ≥ 4 in an initial UnifiedGenotyper run on the full data set as a reference.
515 Genotypes were called on the recalibrated bam files using HaplotypeCaller. Variants were
516 filtered with the following GATK VariantFiltration parameters: QUAL < 100.0, QD < 2.0, MQ <
517 35, FS > 30, HaplotypeScore > 13, MQRankSum < -12.5, ReadPosRankSum < -8. Variants were
518 further filtered with *vcftools*[59] to only retain biallelic SNPs in Hardy-Weinberg equilibrium (p >
519 0.05) with minor allele frequency ≥ 0.1, minimum mean depth of 5, max missing count of 2, and
520 minimum GQ of 99. Finally, SNPs were thinned to a distance of 10 kb basepairs, resulting in a

521 final dataset of 1,965 stringently filtered biallelic SNPs. Missing values were imputed using
522 *beagle*[60], and the resulting vcf file was used to create a kinship matrix using *vcftools*[59]. Values of
523 the kinship matrix were confirmed to be higher in known siblings compared to non-siblings
524 (unpaired t-test, $t = 27.939$, $p = 2.23 \times 10^{-12}$; means = 0.513 and -0.097). Two pairs of siblings
525 were found to have different fathers (G1F022 and G1F025; G4F020 and G4F019).
526
527 **Cell type heterogeneity**
528 Although selection for adherent cells from bone marrow enriches for bMSCs, other cell
529 types are also present[61]. To assess whether cell type heterogeneity accounts for queen-associated
530 differential expression, we used CIBERSORT to deconvolve the proportion of component cell
531 types from the RNA-Seq data[25]. We trained CIBERSORT on a data set of quantile normalized
532 gene expression values from mouse purified primary cell populations[24]. Specifically, we subset
533 the training data to 27 purified cell populations of mesenchymal or hematopoietic origin
534 (Supplementary Figure 3) and to genes that were included in our mole-rat gene expression
535 dataset. We then predicted the composition of the cells that contributed to the mole-rat quantile
536 normalized gene expression data set, for each sample.
537 To test whether cell type heterogeneity was significantly explained by queen status, we
538 also modeled cell type proportion (as summarized by the first principal component of
539 CIBERSORT-estimated proportions for all 27 potential cell types; PC1 explains 50.9% of the
540 overall variation) following the same method used for gene-by-gene expression analysis but with
541 PC1 included as an explanatory variable. We then performed mediation analysis on each of the
542 171 genes that showed a significant effect of breeding status at FDR < 10%. To do so, we first
543 estimated the indirect effect of breeding status on gene expression through the mediating variable
544 (CIBERSORT PC1). The indirect effect of breeding status through CIBERSORT PC1 was
545 estimated by calculating the difference in the effect of breeding status between two models: one
546 model that did not include the mediator (i.e., β_3 and β_4 from equation 1 above) and the same
547 model with the addition of the mediating variable. We performed 1000 iterations of bootstrap
548 resampling to obtain the 95% confidence interval for the indirect effect, and considered an
549 indirect effect for a gene significant if the 95% interval did not overlap 0.
550
551 **ATAC-seq data and transcription factor binding site analysis**
552 To investigate whether differentially expressed genes were associated with accessible
553 binding motifs for specific transcription factors, we generated Omni-ATAC-seq data to profile
554 regions of open chromatin[62,63]. We performed Omni-ATAC-seq on both lumbar vertebrae
555 bMSCs and long bone bMSCs from two female nonbreeding and two queen mole-rats (n = 8
556 libraries total), following the published protocol[63] with the following modifications: 5,000 cells
557 were centrifuged at 500 RCF for 5 minutes at 4°C. The pellet was resuspended in 50 ul
558 transposition mix (25 ul 2xTD buffer, 16.5 ul PBS, 6.75 ul water, 1 ul 10% NP40, 1 ul 10%
559 Tween-20, 1 ul 1% digitonin, and 0.25 ul Tn5 transposase). The reaction was incubated at 37°C
560 for 30 minutes without mixing, followed by a 1.5x Ampure bead cleanup. Omni-ATAC libraries
561 were sequenced on a NovaSeq 6000 as 100 basepair paired-end reads to a mean coverage (± SD)
562 of 26.9 (±4.4) million reads (range: 16.8-38.3). Reads were trimmed with Trim Galore![64] to
563 remove adapter sequence and low quality basepairs (Phred score < 20; reads ≥ 25 bp). Read pairs
564 were mapped to the DMR_v1.0 genome using *bwa-mem*[65] with default settings. Only uniquely
565 mapped reads were retained. The alignment bam files for each treatment (breeding or
566 nonbreeding) were merged, and open chromatin regions were identified using MACS2 v2.1.2[66]

with the following parameters: "-nomodel -keep-dup all -q 0.05". We combined open chromatin peaks with regions in the DMRv1.0 genome that match sequences of vertebrate transcription factor binding site motifs, using motifs defined in the HOMER database[67]. We used Fisher's exact tests (using a p-value threshold of 0.01) to test if transcription factor binding motifs belonging to the same transcription factor were enriched in open chromatin regions within 2,000 bp of the 5' most transcription start site of queen up-regulated genes.

Micro-CT scans and analysis

We performed μCT scans of LV6, LV7, right femur, and right tibia using a VivaCT 80 scanner (Scanco Medical AG, Brüttisellen, Switzerland) set at 55 kVp and 145 μA, with voxel size 10.4 μm. Trabecular bone was quantified from the 100 μCT slices below the proximal tibia growth plate, the 100 μCT slices above the distal femur growth plate, and the 100 μCT slices medial to the caudal growth plate of LV6. To obtain midshaft cross-sections of the femur, tibia, and LV6, we first reduced each bone mesh to 100,000 faces using Avizo Lite version 9.7.0. Mesh files from the same bone type were auto-aligned using Auto3dgm[68] in Matlab. Aligned mesh files were then back scaled to their original sizes in Matlab, and the midshaft cross-section was generated using Rhinoceros version 6. The MomentMacro plugin in ImageJ was used to calculate bone area and moment of inertia.

Classification of breeding status from bone shape

To predict breeding status from bone shape, we first applied the smooth Euler characteristic transform[32] to the aligned right femur and LV6. We then performed leave-one-out predictions, running each bone type separately, using the linear kernel and c-classification with the support vector machine (SVM) implemented by the R package *e1071*[69]. The SVM classifier was equipped with 1:100,000 weighting to achieve class balanced predictions. The empirical p-values were estimated for each bone type by running 100 permutations of the queen/nonbreeder labels[70].

Histochemistry

For a subset of individuals (Supplementary Table 8), the tibia and LV7 were plasticized, sectioned, and stained with Safranin O by the Washington University Musculoskeletal Research Center. The proportion of the tibia proximal growth plate that was fused, and the mean proportion of the LV7 cranial and caudal growth plates that were fused, were measured in ImageJ from Safranin O stained sections. To quantify growth plate activity, we calculated the number of chondrocyte columns (defined as linear stacks of at least three chondrocytes) controlling for length of open growth plate. For each bone type (tibia and LV7), we ran two models: proportion growth plate fusion or chondrocyte columns per mm growth plate as the dependent variable, and number offspring born and age as the independent variables.

Cortical thickness across the femur

We used Stradview[71,72] on dicom images from the μCT scans to measure and visualize, in an automated manner, cortical thickness across the surface of the femur. Bone surface was defined in Stradview by thresholding pixel intensity and contouring the bone at every 14 sections, with the following parameters: resolution = medium, smoothing = standard, strength = very low, contour accuracy = 6. To measure cortical thickness, we used the auto threshold method in Stradview, with line width set to 5, smooth set to 1, and line length set to 3 mm. The

613 smoothed thickness values of each femur were then registered (i.e., mapped) to a single
614 "canonical" femur surface (mole-rat GRF002) using wxRegSurf v18
615 (http://mi.eng.cam.ac.uk/~ahg/wxRegSurf/). We sectioned the cortical thickness values into
616 deciles according to location along the length of the femur. The top and bottom deciles were
617 removed, because cortical and trabecular bone towards the ends of the femur could not be easily
618 differentiated by the automated method. Deciles were then recreated for the remaining length of
619 the bone (i.e., the central 80%). From each bone decile, we estimated cortical thickness as the
620 mean of all cortical thickness measures within that interval. For each decile across animals, we
621 used a linear mixed model to model cortical thickness as a function of breeding status and
622 number offspring, with litter pair as a random effect.
623
624 **Modeling the probability of bone failure**
625 Previous research on mechanical properties of rodent femurs found that, among several
626 morphological and compositional traits measured in eight morphologically varying mouse
627 strains, cortical area (CA) at the midshaft was the best predictor of maximum load (defined as
628 the greatest force attained prior to bone failure, measured via four-point bending; published
629 Pearson's $r = 0.95$)[37]. We therefore used cortical area at the femoral midshaft to predict max load
630 of Damaraland mole-rat femurs. To do so, we first fit a linear model of max load as a function of
631 cortical area (unadjusted for body weight) using published mouse data ($R^2 = 0.877$, n = 81, p =
632 6.64×10^{-38})[37]. We extrapolated from this linear fit to predict max load from cortical area at the
633 midshaft of Damaraland mole-rat femurs. Predicted max loads were then used as input for Cox
634 proportional hazards models, comparing either all queens to nonbreeders or queens with ≥ 6
635 offspring to nonbreeders. Models were fit using the R function *coxph*, and were confirmed to
636 meet the proportional hazards assumption using the *cox.zph* function in the R package *survival*[73].
637 Because max load was not directly measured in the Damaraland mole-rats, we used the Cox
638 proportional hazards models to specifically evaluate the relative hazard of bone failure
639 depending on queen status/number of offspring. We therefore report the results in Figure 6 based
640 on relative force (with the median predicted failure value for nonbreeders set to 1) instead of
641 absolute force in Newtons.
642
643 **Data Availability**
644 All RNA sequencing data generated during this study are available in the NCBI Gene Expression
645 Omnibus (series accession GSE152659). ATAC-Seq data are available in the NCBI Sequence
646 Read Archive (BioProject accession number PRJNA649596). µCT data from this study are
647 available on MorphoSource (http://www.morphosource.org, project 1056).
648

References

1 Wilson, E. O. The insect societies. *The insect societies.* (1971).

2 Keller, L. & Genoud, M. Extraordinary lifespans in ants: a test of evolutionary theories of ageing. *Nature* **389**, 958-960 (1997).

3 Berndt, K. P. & Eichler, W. Die Pharaoameise, Monomorium pharaonis (L.)(Hym., Myrmicidae). *Mitteilungen aus dem Museum für Naturkunde in Berlin. Zoologisches Museum und Institut für Spezielle Zoologie (Berlin)* **63**, 3-186 (1987).

4 Page Jr, R. E. & Peng, C. Y.-S. Aging and development in social insects with emphasis on the honey bee, Apis mellifera L. *Experimental gerontology* **36**, 695-711 (2001).

5 Smith, C. R., Toth, A. L., Suarez, A. V. & Robinson, G. E. Genetic and genomic analyses of the division of labour in insect societies. *Nature Reviews Genetics* **9**, 735-748 (2008).

6 Koenig, W. D. & Dickinson, J. L. *Cooperative breeding in vertebrates: studies of ecology, evolution, and behavior*. (Cambridge University Press, 2016).

7 Clutton-Brock, T. *et al.* Intrasexual competition and sexual selection in cooperative mammals. *Nature* **444**, 1065-1068 (2006).

8 Huchard, E., English, S., Bell, M. B., Thavarajah, N. & Clutton-Brock, T. Competitive growth in a cooperative mammal. *Nature* **533**, 532-534 (2016).

9 O'Riain, M., Jarvis, J., Alexander, R., Buffenstein, R. & Peeters, C. Morphological castes in a vertebrate. *Proceedings of the National Academy of Sciences* **97**, 13194-13197 (2000).

10 Russell, A. F., Carlson, A. A., McIlrath, G. M., Jordan, N. R. & Clutton‐Brock, T. Adaptive size modification by dominant female meerkats. *Evolution* **58**, 1600-1607 (2004).

11 Thorley, J., Katlein, N., Goddard, K., Zöttl, M. & Clutton-Brock, T. Reproduction triggers adaptive increases in body size in female mole-rats. *Proceedings of the Royal Society B: Biological Sciences* **285**, 20180897 (2018).

12 Young, A. J. & Bennett, N. C. Morphological divergence of breeders and helpers in wild Damaraland mole‐rat societies. *Evolution: International Journal of Organic Evolution* **64**, 3190-3197 (2010).

13 Bens, M. *et al.* Naked mole-rat transcriptome signatures of socially suppressed sexual maturation and links of reproduction to aging. *BMC biology* **16**, 77 (2018).

14 Mulugeta, E. *et al.* Molecular insights into the pathways underlying naked mole-rat eusociality. *bioRxiv*, 209932 (2017).

15 Sahm, A. *et al.* Status-dependent aging rates in long-lived, social mole-rats are shaped by HPA stress axis. *bioRxiv* (2020).

16 Bennett, N. C. & Faulkes, C. G. *African mole-rats: ecology and eusociality*. (Cambridge University Press, 2000).

17 Jarvis, J. Eusociality in a mammal: cooperative breeding in naked mole-rat colonies. *Science* **212**, 571-573 (1981).

18 Jarvis, J. & Bennett, N. Eusociality has evolved independently in two genera of bathyergid mole-rats—but occurs in no other subterranean mammal. *Behavioral Ecology and Sociobiology* **33**, 253-260 (1993).

19 Bennett, N., Faulkes, C. & Molteno, A. Reproductive suppression in subordinate, non-breeding female Damaraland mole-rats: two components to a lifetime of socially

694 induced infertility. *Proceedings of the Royal Society of London. Series B: Biological*
695 *Sciences* **263**, 1599-1603 (1996).
696 20 Snyman, P., Jackson, C. R. & Bennett, N. C. Do dispersing non-reproductive female
697 Damaraland mole-rats, Cryptomys damarensis (Rodentia: Bathyergidae) exhibit
698 spontaneous or induced ovulation? *Physiology & behavior* **87**, 88-94 (2006).
699 21 Henry, E. C., Dengler-Crish, C. M. & Catania, K. C. Growing out of a caste-reproduction
700 and the making of the queen mole-rat. *Journal of Experimental Biology* **210**, 261-268
701 (2007).
702 22 Dengler‐Crish, C. M. & Catania, K. C. Cessation of reproduction‐related spine
703 elongation after multiple breeding cycles in female naked mole‐rats. *The*
704 *Anatomical Record: Advances in Integrative Anatomy and Evolutionary Biology:*
705 *Advances in Integrative Anatomy and Evolutionary Biology* **292**, 131-137 (2009).
706 23 Dominici, M. *et al.* Minimal criteria for defining multipotent mesenchymal stromal
707 cells. The International Society for Cellular Therapy position statement. *Cytotherapy*
708 **8**, 315-317 (2006).
709 24 Hume, D. A., Summers, K. M., Raza, S., Baillie, J. K. & Freeman, T. C. Functional
710 clustering and lineage markers: insights into cellular differentiation and gene
711 function from large-scale microarray studies of purified primary cell populations.
712 *Genomics* **95**, 328-338 (2010).
713 25 Newman, A. M. *et al.* Robust enumeration of cell subsets from tissue expression
714 profiles. *Nature methods* **12**, 453 (2015).
715 26 Redlich, K. & Smolen, J. S. Inflammatory bone loss: pathogenesis and therapeutic
716 intervention. *Nature reviews Drug discovery* **11**, 234-250 (2012).
717 27 Darden, A. G., Ries, W. L., Wolf, W. C., Rodriguiz, R. M. & Key Jr, L. L. Osteoclastic
718 superoxide production and bone resorption: stimulation and inhibition by
719 modulators of NADPH oxidase. *Journal of Bone and Mineral Research* **11**, 671-675
720 (1996).
721 28 Datta, H., Rathod, H., Manning, P., Turnbull, Y. & McNeil, C. Parathyroid hormone
722 induces superoxide anion burst in the osteoclast: evidence for the direct
723 instantaneous activation of the osteoclast by the hormone. *Journal of endocrinology*
724 **149**, 269-275 (1996).
725 29 Key, L., Ries, W., Taylor, R., Hays, B. & Pitzer, B. Oxygen derived free radicals in
726 osteoclasts: the specificity and location of the nitroblue tetrazolium reaction. *Bone*
727 **11**, 115-119 (1990).
728 30 Key, L., Wolf, W., Gundberg, C. & Ries, W. Superoxide and bone resorption. *Bone* **15**,
729 431-436 (1994).
730 31 Segeletz, S. & Hoflack, B. Proteomic approaches to study osteoclast biology.
731 *Proteomics* **16**, 2545-2556 (2016).
732 32 Crawford, L., Monod, A., Chen, A. X., Mukherjee, S. & Rabadán, R. Functional data
733 analysis using a topological summary statistic: the smooth Euler characteristic
734 transform. *arXiv preprint arXiv:1611.06818* (2016).
735 33 Kilborn, S. H., Trudel, G. & Uhthoff, H. Review of growth plate closure compared with
736 age at sexual maturity and lifespan in laboratory animals. *Journal of the American*
737 *Association for Laboratory Animal Science* **41**, 21-26 (2002).

34 Kovacs, C. S. Maternal mineral and bone metabolism during pregnancy, lactation, and post-weaning recovery. *Physiological reviews* **96**, 449-547 (2016).

35 Schmidt, C. M., Jarvis, J. U. & Bennett, N. C. The long-lived queen: reproduction and longevity in female eusocial Damaraland mole-rats (Fukomys damarensis). *African Zoology* **48**, 193-196 (2013).

36 Szulc, P., Seeman, E., Duboeuf, F., Sornay‐Rendu, E. & Delmas, P. D. Bone fragility: failure of periosteal apposition to compensate for increased endocortical resorption in postmenopausal women. *Journal of bone and mineral research* **21**, 1856-1863 (2006).

37 Jepsen, K. J., Akkus, O. J., Majeska, R. J. & Nadeau, J. H. Hierarchical relationship between bone traits and mechanical properties in inbred mice. *Mammalian Genome* **14**, 97-104 (2003).

38 Rodrigues, M. A. & Flatt, T. Endocrine uncoupling of the trade-off between reproduction and somatic maintenance in eusocial insects. *Current opinion in insect science* **16**, 1-8 (2016).

39 Rueppell, O., Aumer, D. & Moritz, R. F. Ties between ageing plasticity and reproductive physiology in honey bees (Apis mellifera) reveal a positive relation between fecundity and longevity as consequence of advanced social evolution. *Current opinion in insect science* **16**, 64-68 (2016).

40 Houslay, T. M., Vullioud, P., Zöttl, M. & Clutton-Brock, T. H. Benefits of cooperation in captive Damaraland mole-rats. *Behavioral Ecology* (2020).

41 Clutton-Brock, T. H. & Manser, M. Meerkats: cooperative breeding in the Kalahari. *Cooperative breeding in vertebrates* **294**, 317 (2016).

42 Rosa, N., Simoes, R., Magalhães, F. D. & Marques, A. T. From mechanical stimulus to bone formation: a review. *Medical engineering & physics* **37**, 719-728 (2015).

43 Jarvis, J. U., O'Riain, M. J., Bennett, N. C. & Sherman, P. W. Mammalian eusociality: a family affair. *Trends in Ecology & Evolution* **9**, 47-51 (1994).

44 Pinto, M., Jepsen, K., Terranova, C. & Buffenstein, R. Lack of sexual dimorphism in femora of the eusocial and hypogonadic naked mole-rat: a novel animal model for the study of delayed puberty on the skeletal system. *Bone* **46**, 112-120 (2010).

45 Schneider, C. A., Rasband, W. S. & Eliceiri, K. W. NIH Image to ImageJ: 25 years of image analysis. *Nature methods* **9**, 671-675 (2012).

46 Martin, M. Cutadapt removes adapter sequences from high-throughput sequencing reads. *EMBnet. journal* **17**, 10-12 (2011).

47 Fang, X. *et al.* Adaptations to a subterranean environment and longevity revealed by the analysis of mole rat genomes. *Cell reports* **8**, 1354-1364 (2014).

48 Dobin, A. *et al.* STAR: ultrafast universal RNA-seq aligner. *Bioinformatics* **29**, 15-21 (2013).

49 Anders, S., Pyl, P. T. & Huber, W. HTSeq–A Python framework to work with high-throughput sequencing data. *Bioinformatics*, btu638 (2014).

50 Wagner, G. P., Kin, K. & Lynch, V. J. Measurement of mRNA abundance using RNA-seq data: RPKM measure is inconsistent among samples. *Theory in biosciences* **131**, 281-285 (2012).

51 Law, C. W., Chen, Y., Shi, W. & Smyth, G. K. Voom: precision weights unlock linear model analysis tools for RNA-seq read counts. *Genome biology* **15**, R29 (2014).

783 52 Robinson, M. D. & Oshlack, A. A scaling normalization method for differential
784 expression analysis of RNA-seq data. *Genome biology* **11**, R25 (2010).
785 53 Anders, S. & Huber, W. Differential expression analysis for sequence count data.
786 *Genome Biol* **11**, R106, doi:10.1186/gb-2010-11-10-r106 (2010).
787 54 Smyth, G. K. in *Bioinformatics and computational biology solutions using R and*
788 *Bioconductor* 397-420 (Springer, 2005).
789 55 Akdemir, D. & Okeke, U. EMMREML: Fitting mixed models with known covariance
790 structures. *R package version* **3** (2015).
791 56 Storey, J. D. & Tibshirani, R. Statistical significance for genomewide studies. *Proc*
792 *Natl Acad Sci U S A* **100**, 9440-9445, doi:10.1073/pnas.1530509100 (2003).
793 57 Raudvere, U. *et al.* g: Profiler: a web server for functional enrichment analysis and
794 conversions of gene lists (2019 update). *Nucleic acids research* **47**, W191-W198
795 (2019).
796 58 McKenna, A. *et al.* The Genome Analysis Toolkit: a MapReduce framework for
797 analyzing next-generation DNA sequencing data. *Genome research* **20**, 1297-1303
798 (2010).
799 59 Danecek, P. *et al.* The variant call format and VCFtools. *Bioinformatics* **27**, 2156-
800 2158 (2011).
801 60 Browning, S. R. & Browning, B. L. Rapid and accurate haplotype phasing and
802 missing-data inference for whole-genome association studies by use of localized
803 haplotype clustering. *The American Journal of Human Genetics* **81**, 1084-1097
804 (2007).
805 61 Phinney, D. G., Kopen, G., Isaacson, R. L. & Prockop, D. J. Plastic adherent stromal
806 cells from the bone marrow of commonly used strains of inbred mice: variations in
807 yield, growth, and differentiation. *Journal of cellular biochemistry* **72**, 570-585
808 (1999).
809 62 Buenrostro, J. D., Giresi, P. G., Zaba, L. C., Chang, H. Y. & Greenleaf, W. J. Transposition
810 of native chromatin for fast and sensitive epigenomic profiling of open chromatin,
811 DNA-binding proteins and nucleosome position. *Nature methods* **10**, 1213 (2013).
812 63 Corces, M. R. *et al.* An improved ATAC-seq protocol reduces background and enables
813 interrogation of frozen tissues. *Nature methods* **14**, 959 (2017).
814 64 Krueger, F. Trim Galore.
815 http://www.bioinformatics.babraham.ac.uk/projects/trim_galore/ (2015).
816 65 Li, H. & Durbin, R. Fast and accurate long-read alignment with Burrows–Wheeler
817 transform. *Bioinformatics* **26**, 589-595 (2010).
818 66 Zhang, Y. *et al.* Model-based analysis of ChIP-Seq (MACS). *Genome biology* **9**, R137
819 (2008).
820 67 Heinz, S. *et al.* Simple combinations of lineage-determining transcription factors
821 prime cis-regulatory elements required for macrophage and B cell identities.
822 *Molecular cell* **38**, 576-589 (2010).
823 68 Boyer, D. M. *et al.* A new fully automated approach for aligning and comparing
824 shapes. *The Anatomical Record* **298**, 249-276 (2015).
825 69 Dimitriadou, E., Hornik, K., Leisch, F., Meyer, D. & Weingessel, A. Misc functions of
826 the Department of Statistics (e1071), TU Wien. *R package* **1**, 5-24 (2008).

70 Golland, P., Liang, F., Mukherjee, S. & Panchenko, D. Permutation tests for classification. *International Conference on Computational Learning Theory*, 501-515 (2005).

71 Treece, G. M. http://mi.eng.cam.ac.uk/~gmt11/stradview. (2019).

72 Treece, G. M., Gee, A. H., Mayhew, P. & Poole, K. E. High resolution cortical bone thickness measurement from clinical CT data. *Medical image analysis* **14**, 276-290 (2010).

73 Therneau, T. M. A Package for Survival Analysis in R. R package version 3.1-12, available at https://CRAN.R-project.org/package=survival. (2020).

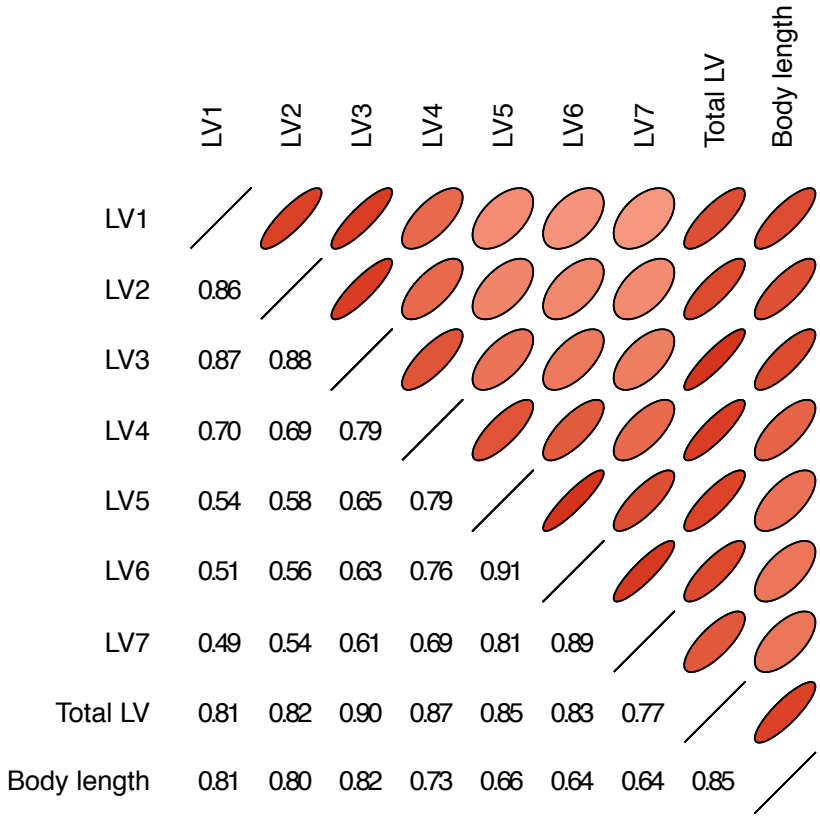

Supplementary Figure 1. Body length is positively correlated with the lengths of lumbar vertebrae (LV) 1 - 7. Pearson correlations between the length of each lumbar vertebra and body length from mole-rat x-ray data. Narrower ovals with darker shades of red indicate larger Pearson correlations; correlation values are also given in the lower left triangle.

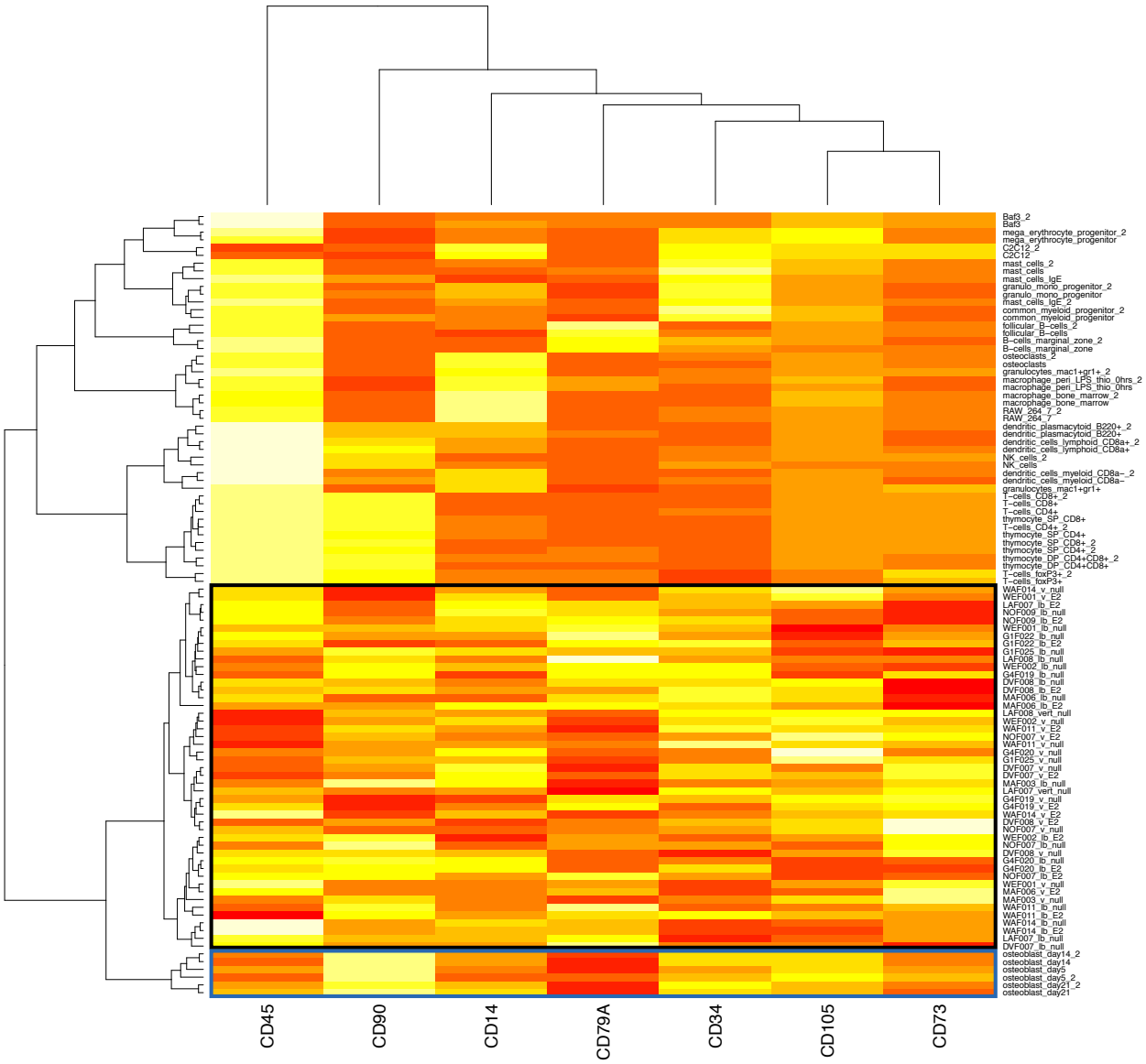

843 **Supplementary Figure 2. Mole-rat RNA-Seq samples cluster closest with purified mouse**
844 **osteoblasts, based on canonical bMSC markers.** Clustering was performed using Ward's
845 hierarchical clustering method on Euclidean distances of the quantile normalized expression of
846 the seven bMSC markers (out of 11 described[23]) that were quantified in both the mole-rat and
847 reference mouse[24] data sets. The black box indicates mole-rat samples, and the blue box indicates
848 mouse osteoblasts, a bMSC lineage cell type.
849

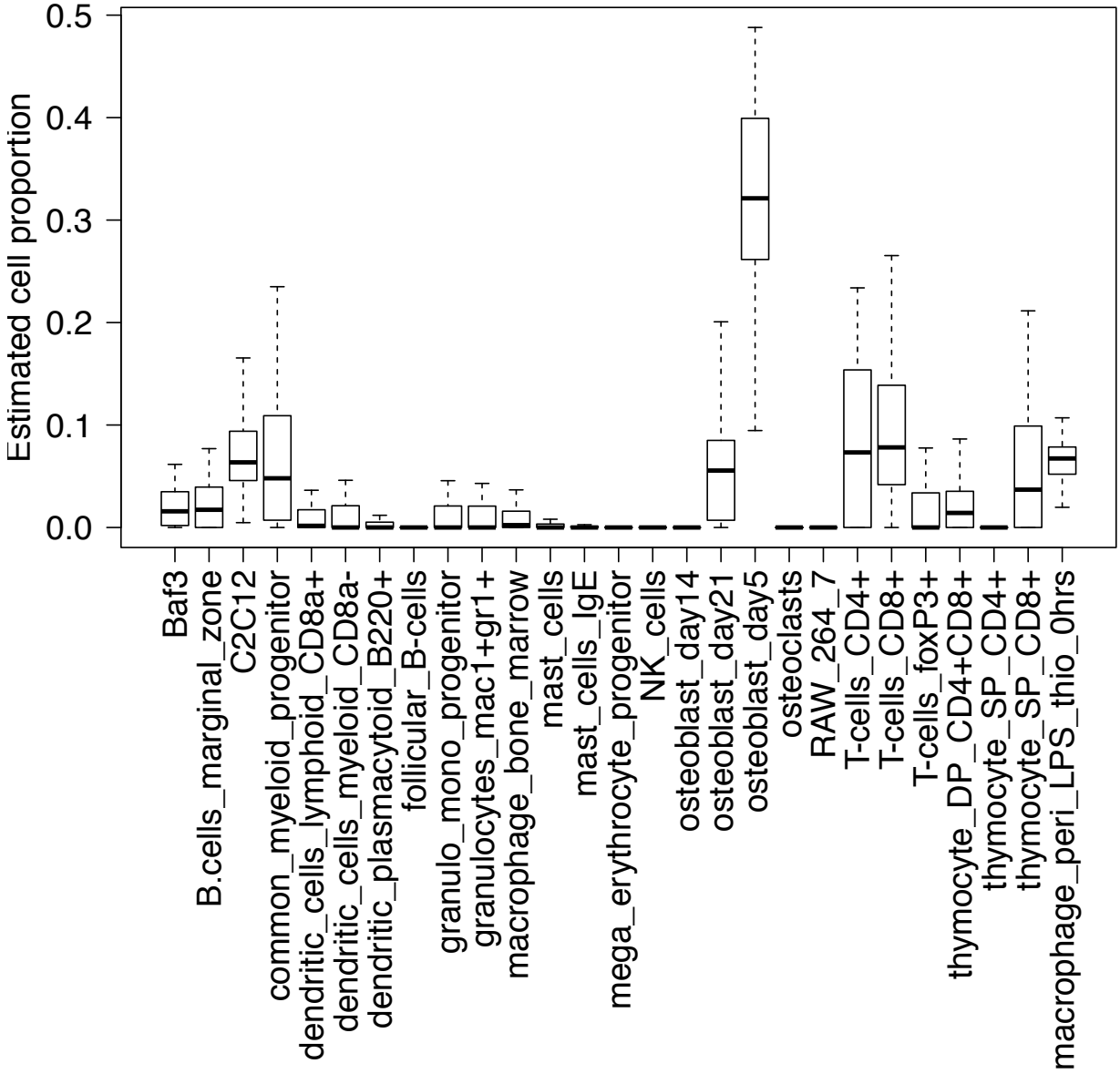

Supplementary Figure 3. Estimated cell proportions for the 47 mole-rat RNA-Seq samples. Each box represents the interquartile range, with the median value depicted as a horizontal bar. Whiskers extend to the most extreme estimates within 1.5x the interquartile range. Cell proportions were estimated with CIBERSORT[25], based on reference gene expression levels for 412 marker genes in 27 purified mouse cell types[24]. The predicted predominant cell type in the mole-rat samples is most similar to early stage osteoblasts, which are cells from the bMSC lineage.

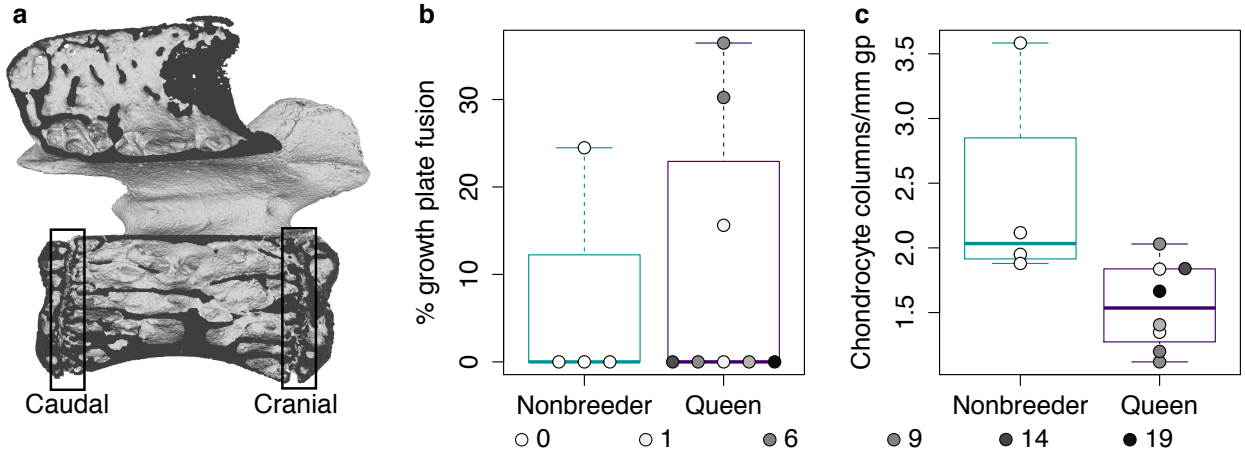

Supplementary Figure 4. Growth potential in lumbar vertebra 7 (LV7). (a) µCT scan of LV7 of a female Damaraland mole-rat. The boxes indicate the locations of the caudal and cranial growth plates. (b) The number of offspring produced by queens does not significantly predict growth plate fusion (quantified as the average of the caudal and cranial growth plates; $\beta = 2.745 \times 10^{-4}$, $p = 0.970$, $n = 12$, controlling for age) or chondrocyte proliferation within the remaining growth plate ($\beta = -0.033$, $p = 0.293$, $n = 12$, controlling for age). Each box represents the interquartile range, with the median value depicted as a horizontal bar. Whiskers extend to the most extreme values within 1.5x of the interquartile range. Dots represent individual animals, and shading indicates each animal's total offspring number.

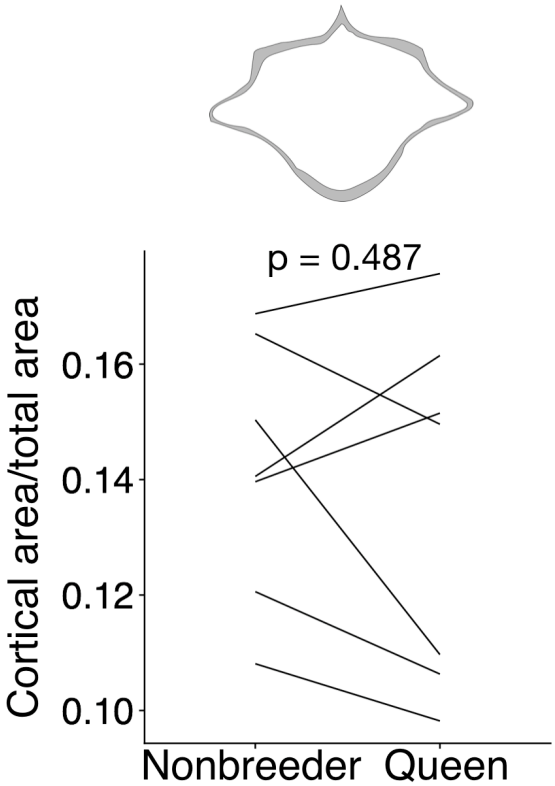

Supplementary Figure 5. Queens do not exhibit reduced cortical area at the midsection of LV6. At top, cross-section with area highlighted in gray shows the measure represented in the plot. Each line represents an age-matched nonbreeder and queen littermate pair. Queens and nonbreeders show no difference in cortical area/total area at the LV6 midsection (paired t-test of cortical area/total area, t = -0.741, df = 6, p = 0.487).

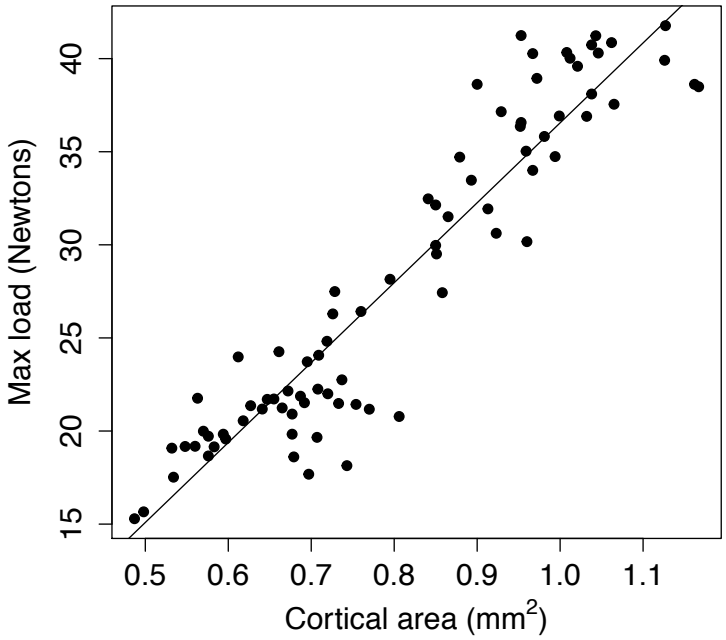

Supplementary Figure 6. Relationship between max load and cortical area in mouse femurs. Max load shows a highly linear relationship with cortical area across mouse femurs ($R^2 = 0.88$, $p = 6.64 \times 10^{-38}$). Each dot represents a single mouse femur. Solid line indicates the best fit line. Data are from [37].